1   **Title:**

2   Altered *N*-glycan composition impacts flagella mediated adhesion in *Chlamydomonas*

3   *reinhardtii*

4   **Authors:**

5   Nannan Xu[1,2]*, Anne Oltmanns[3]*, Longsheng Zhao[4,5], Antoine Girot[6], Marzieh Karimi[6], Lara

6   Hoepfner[3], Simon Kelterborn[7], Martin Scholz[3], Julia Beißel[3], Peter Hegemann[7], Oliver

7   Bäumchen[6], Luning N. Liu[4,8], Kaiyao Huang[1#], Michael Hippler[3,9#]

8   **Affiliations:**

9   [1]Key Laboratory of Algal Biology, Institute of Hydrobiology, Chinese Academy of Sciences,

10   Wuhan, Hubei 430072, China

11   [2]University of Chinese Academy of Sciences, Beijing 100049, China

12   [3]Institute for Plant Biology and Biotechnology, University of Münster, 48143 Münster,

13   Germany

14   [4]Institute of Integrative Biology, University of Liverpool, Liverpool L69 7ZB, United

15   Kingdom

16   [5]State Key Laboratory of Microbial Technology, and Marine Biotechnology Research Center,

17   Shandong University, Qingdao 266237, China

18   [6]Max Planck Institute for Dynamics and Self-Organization (MPIDS), 37077 Göttingen,

19   Germany

20   [7]Institute of Biology, Experimental Biophysics, Humboldt University of Berlin, 10099 Berlin,

21   Germany

22   [8]College of Marine Life Sciences, and Frontiers Science Center for Deep Ocean Multispheres

23   and Earth System, Ocean University of China, Qingdao 266003, China

24   [9]Institute of Plant Science and Resources, Okayama University, Kurashiki 710-0046, Japan.

25

26   **Corresponding authors**:

27   Kaiyao Huang; huangky@ihb.ac.cn; Tel. +86-27-68780901

28   Michael Hippler; mhippler@uni-muenster.de; Tel. +49 251 83-24790

29   **Short title:**

30   *N*-glycosylation impacts adhesion in *Chlamydomonas*

31   **Abstract**

32   For the unicellular alga *Chlamydomonas reinhardtii,* the presence of *N*-glycosylated proteins

33   on the surface of two flagella is crucial for both cell-cell interaction during mating and flagellar

34   surface adhesion. It is unknown whether the composition of *N*-glycans attached to respective

35   proteins is important for these processes. To this end, we examined several *C. reinhardtii*

36   insertional mutants and a CRIPSR/Cas9 knockout mutant of xylosyltransferase 1A, all

37   possessing altered *N*-glycan compositions. Taking advantage of atomic force microscopy and

38   micropipette force measurements, our data revealed that reduction in *N*-glycan complexity

39   impedes the adhesion force required for binding the flagella to surfaces. In addition, polystyrene

40   bead binding and transport is impaired. Notably, assembly, Intraflagellar Transport and FMG-

41   1B transport into flagella are not affected by altered *N*-glycosylation. Thus, we conclude that

42   proper *N*-glycosylation of flagellar proteins is crucial for adhering *C. reinhardtii* cells onto

43   surfaces, indicating that *N*-glycans mediate surface adhesion via direct surface contact.

44   **Keywords**

45   adhesion/ AFM/ C reinhardtii/ flagella/ N-glycosylation

46   **Introduction**

47   *N*-glycosylation, as one of the major post-translational modifications, takes place along the

48   ER/Golgi secretion route and consequently most *N*-linked glycans are found on proteins facing

49   the extracellular space. Initial steps of *N*-glycosylation in the ER are highly conserved among

50   most eukaryotes and consist of the synthesis of a common prebuilt *N*-glycan precursor onto a

51   dolichol phosphate. Following the transfer of the glycan precursor onto the asparagine of the

52 consensus sequence N-X-S/T of a nascent protein (where X can be any amino acid except

53 proline), the glycoprotein is folded by the glycan recognizing chaperones Calnexin and

54 Calreticulin (Stanley P, Taniguchi N, 2017). Subsequent *N*-glycan maturation steps in the Golgi

55 are species dependent and gives rise to a high variety of *N*-glycan structures. In land plants,

56 Golgi maturation leads to *N*-glycans modified with β1,2-core xylose and α1,3-core fucose

57 (Strasser, 2016). In *Chlamydomonas reinhardtii*, a unicellular biflagellate green alga, *N*-glycans

58 can be decorated with core xylose and -fucose (Lucas et al., 2020; Oltmanns et al., 2020;

59 Schulze et al., 2018). Additionally, *6O*-methylation of mannose and addition of a terminally

60 linked β1,4-xylose were reported (Mathieu-Rivet et al., 2013). While the functional advantage

61 of *N*-linked glycans of mature proteins is hardly understood, it is known that blocking the

62 synthesis of a full *N*-glycan precursor results in hypoglycosylated proteins that cannot be folded

63 properly (Gardner et al., 2013). Instead, they are degraded via the ER-associated degradation

64 pathway (ERAD) and are consequently not targeted correctly (Adams et al., 2019; Cherepanova

65 et al., 2016). Therefore, impairment of glycosylation at such early stage is lethal in both uni- and

66 multicellular organisms and only when inhibition of glycosylation is carefully dosed (e.g. by

67 tunicamycin), immediate physiological effects caused by hypoglycosylation can be observed

68 (Kukuruzinska et al., 1987). Looking at *C. reinhardtii*, treatment of vegetative cells with

69 tunicamycin lead to an impaired flagellar adhesiveness, indicating that glycoproteins are crucial

70 for adhesion and the subsequent onset of gliding (Bloodgood, 1987). However, whether this

71 phenotype is linked to lack of proteins and/or the of lack *N*-glycosylation is unclear.

72 Whole cell gliding is one of two flagella based motilities in *C. reinhardtii* besides swimming

73 (Ishikawa and Marshall, 2011; Kozminski et al., 1993; Snell et al., 2004). In principle, the cell

74 adheres to a surface via its flagella, positioning them in a 180° angle and starts gliding along

75 the solid or semisolid surface into the direction in which one flagellum is pointing (designating

76 it as leading flagellum) (Bloodgood, 2009). Interestingly, flagella not only bind to large solid

77   surfaces, but they also bind to small, inert objects (e.g. polystyrene microbeads) that are moved

78   along the flagellar membrane. While the two events are believed to underly the same molecular

79   machinery, it is assumed that they start with an adhesion of flagella membrane components to

80   the surface (Bloodgood and Salomonsky, 1998). A micropipette force measurement approach

81   recently showed that the flagella adhesion forces on different model surfaces with tailored

82   properties lie in the range of 1 to 4 nN and that only positive surface charge diminished the

83   adhesion force significantly (Backholm and Bäumchen, 2019; Kreis et al., 2019, 2018).

84   Remarkably, surface iodination experiments in the early 1980s revealed a single protein called

85   flagellar membrane glycoprotein 1B (FMG-1B) as the main player mediating surface contact

86   (Bloodgood and Workman, 1984). FMG-1B is exclusively located in the flagellar membrane

87   and has a remarkable size of around 350 kDa (4389 amino acids) with a large extra-flagellar

88   part (4340 amino acids) anchored in the membrane via an expected single trans membrane

89   helix of 22 amino acids (Bloodgood et al., 2019). As the name indicates, it is heavily *N-* and *O-*

90   glycosylated. A recent knock down study showed, that it is the main constituent of the

91   glycocalyx surrounding the flagellum. Additionally, a *fmg-1B* mutant showed a drastically

92   reduced ability to glide (Bloodgood et al., 2019). Strikingly, FMG-1B is present at a high copy

93   number and turns over rapidly within approximately 1 h (Bloodgood, 2009). The rapid turnover

94   is probably attributed to the fact that flagellar membrane components are constantly shed into

95   the medium as flagellar ectosomes (Bloodgood, 2009; Wood et al., 2013). FMG-1B and another

96   *N*-glycosylated membrane component, FAP113, have been shown to be eventually torn out of

97   the membrane once bound to microbeads (Kamiya et al., 2018). Whether FAP113 is only

98   involved in microbead binding or also in whole cell gliding is unknown.

99   Recently, it was found that the flagella adhesion to surfaces is switchable by light, indicating

100   that a blue-light photoreceptor signal is underlying this process.[18] Following adhesion to the

101   surface, a transmembrane signal mediates translation of the adhesion event into a calcium

4

102   transient and protein phosphorylation cascade (Bloodgood, 2009; Collingridge et al., 2013;

103   Kreis et al., 2018). According to the current model, an interaction of the short cytoplasmic part

104   of FMG-1B with Intraflagellar Transport (IFT) may occur (Laib et al., 2009; Shih et al., 2013).

105   IFT moves bidirectionally along the flagellar microtubules, the anterograde transport is driven

106   by kinesin 2 and retrograde transport is driven by cytoplasmic dynein-1b (Cole et al., 1998;

107   Huangfu et al., 2003; Kozminski et al., 1995; Lechtreck, 2015; Pedersen and Rosenbaum, 2008;

108   Porter et al., 1999; Rosenbaum and Witman, 2002). Since retrograde motor dynein-1b pauses

109   relative to the adhesion site while FMG-1B tethers to the solid surface through its large

110   extracellular carbohydrate domain (Bloodgood, 2009), the force generated by motor proteins

111   will push the microtubule into the opposite direction, dragging the cell body and the second

112   flagellum behind; the gliding process is initiated (Shih et al., 2013).

113   Considering that *N*-glycoproteins *per se* are important for adhesion but are constantly lost from

114   the flagellar membrane, gliding is supposed to require an enormous amount of energy, which

115   suggests that flagella mediated adhesion has a somewhat high importance. Furthermore, it

116   opens the question whether the maturation of *N*-glycans (as additional energy expense) in Golgi

117   is important for flagella mediated adhesion, i.e. whether *N*-glycosylation is crucial for adhesion

118   beyond proper glycoprotein folding. Therefore, we compared flagellar membrane motility of

119   different mutant strains impaired in *N*-glycan maturation (characterized in Schulze *et al.* 2018).

120   We found that *N*-glycan maturation indeed impacts the interaction of flagellum and surface in

121   all mutants analyzed.

122   **Results**

123   **Altered *N*-linked glycans do not change the flagellar localization of FMG-1B**

124   To test whether *N*-glycan maturation in Golgi is important for flagella surface motility in

125   *C. reinhardtii*, two insertional mutants such as IM_{Man1A}, IM_{XylT1A} and their double mutant

5

126   IM$_{Man1A}$xIM$_{XylT1A}$ were used. Initially, these mutants had been described in Schulze *et al.* 2018,

127   where *N*-glycan patterns of supernatant proteins were analyzed and compared (Fig. 1A). The

128   insertional mutagenesis giving rise to these mutants was performed in the parental strain CC-

129   4375 (a *ift46* mutant backcrossed with CC124) complemented with IFT-46::YFP referred to as

130   WT-Ins throughout the current study. The first mutant, deficient in xylosyltransferase 1A

131   (IM$_{XylT1A}$), produces *N*-glycans devoid of core xylose while simultaneously having a reduced

132   length. Second mutant IM$_{Man1A}$, a knock down mutant of mannosidase 1A, is mainly

133   characterized by a lack of 6*O*-methylation of mannose residues while the *N*-glycan length is

134   slightly greater than in WT-Ins. Furthermore, *N*-glycans of IM$_{Man1A}$ are slightly reduced in

135   terminal xylose and core fucose. Finally, a double mutant of the above two single mutants

136   (IM$_{Man1A}$xIM$_{XylT1A}$, obtained by genetic crossing) produces *N*-glycans devoid of 6*O*-

137   methylation but of WT-Ins length and carrying core xylose and fucose residues (Fig. 1A). It is

138   of note that in none of the mutants the flagellar length is altered as compared to WT-Ins (Figure

139   1 - Supplementary Fig. 1). To confirm that flagellar *N*-glycan patterns of these mutants deviate

140   from WT-Ins, whole cell extracts and isolated flagella were probed with anti-HRP, which is

141   specifically binding to β1,2-xylose and α1,3-fucose attached to the *N*-glycan core (Kaulfürst-

142   Soboll et al., 2011). In line with previous publications, the antibody showed a higher affinity

143   towards *N*-glycoproteins synthesized by IM$_{Man1A}$ and IM$_{Man1A}$xIM$_{XylT1A}$ while it showed a

144   decreased affinity towards probes of IM$_{XylT1A}$ (Figure 1 - Supplementary Fig. 2) (Schulze et al.,

145   2018).

146   Since FMG-1B is the major constituent of the flagellar glycoproteome and to date is the only

147   protein proven to be involved in flagellar surface motility, different monoclonal antibodies

148   raised against FMG-1B were employed to analyze FMG1-B localization (Bloodgood et al.,

149   1986; Long et al., 2016). The whole cell or isolated flagella from IM$_{Man1A}$, IM$_{XylT1A}$ and their

150   double mutant IM$_{Man1A}$xIM$_{XylT1A}$ were probed separately with the glycan epitope recognizing

6

151 antibody or the antibody against the peptide epitope of FMG-1B. Both antibodies gave strong

152 signals in WT-Ins and WT-CC-124 (WT-CC-124 is minus gamete used to cross with mutants)

153 (Fig. 1B). On the contrary, the glycan specific antibody showed low affinity towards FMG-1B

154 in cell body and flagella of IM_{Man1A}, IM_{XylT1A} and the double mutant, proving that N-

155 glycosylation of FMG-1B is altered in respective strains (Fig. 1B). Additionally, mass

156 spectrometric analyses of intact N-glycopeptides derived from the flagella of these mutants

157 confirmed that the change of flagellar N-glycan composition is similar to the previously

158 reported composition of N-linked glycans among supernatant proteins (Figure 1-

159 Supplementary Fig. 3) (Schulze et al., 2018). Conversely, the antibody specifically binding to

160 the peptide backbone of FMG-1B resulted in signals comparable to WT-Ins for all mutants

161 analyzed. In addition, label free mass spectrometric quantification confirmed that FMG-1B is

162 correctly targeted to the flagella in all mutants analyzed (Fig. 1B and C). The same is true for

163 FAP113, another protein shown to be involved in flagella surface motility (Fig. 1D).

164 To compare the localization of glycan and protein of FMG-1B in WT-Ins and mutants,

165 IFT46::YFP was removed from the IM strains by crossing the mutant with WT-CC124. The

166 obtained progenies of IM_{Man1A}, IM_{XylT1A} and IM_{Man1A}xIM_{XylT1A} did not express IFT46::YFP

167 (Figure 1 - Supplementary Fig. 4). For imaging, these mutants were mixed with an equal amount

168 of WT-Ins cells and incubated with FMG-1B glycan- or peptide specific antibodies. In the

169 mixed sample of WT-Ins with IM_{Man1A}, a uniform signal of the glycan specific antibody was

170 found in the flagella and cell wall of WT-Ins. At the same time no glycan signal was observed

171 for the flagella of IM_{Man1A} and the signal in the cell wall of IM_{Man1A} was very weak. It must be

172 noted, that cross reaction of the N-glycan specific antibody with cell wall localized glycosylated

173 proteins has been reported previously.(Bloodgood et al., 1986) On the other hand, the FMG-1B

174 peptide signal concentrated in the flagella of both WT-Ins and IM_{Man1A} (Fig. 1E, first column).

175 Similar to IM_{Man1A}, the glycan signal was not detected in flagella of IM_{XylT1A} and the double

7

176   mutant, while the FMG-1B peptide signal was clearly present in the flagella of these two

177   mutants (Fig. 1E, second and third columns). All these data showed that altered *N*-glycan

178   maturation did not affect the flagellar localization of FMG-1B. Although FMG-1B is the most

179   prominent and best studied flagella membrane glycoprotein, there might be other glycoproteins

180   involved in flagellar adhesion. Nevertheless, no protein was found consistently and

181   significantly changed in abundance in flagella of the IM strains analyzed when compared to

182   WT-Ins (Figure 1 - Supplementary Fig. 5), also indicating that flagellar assembly is not

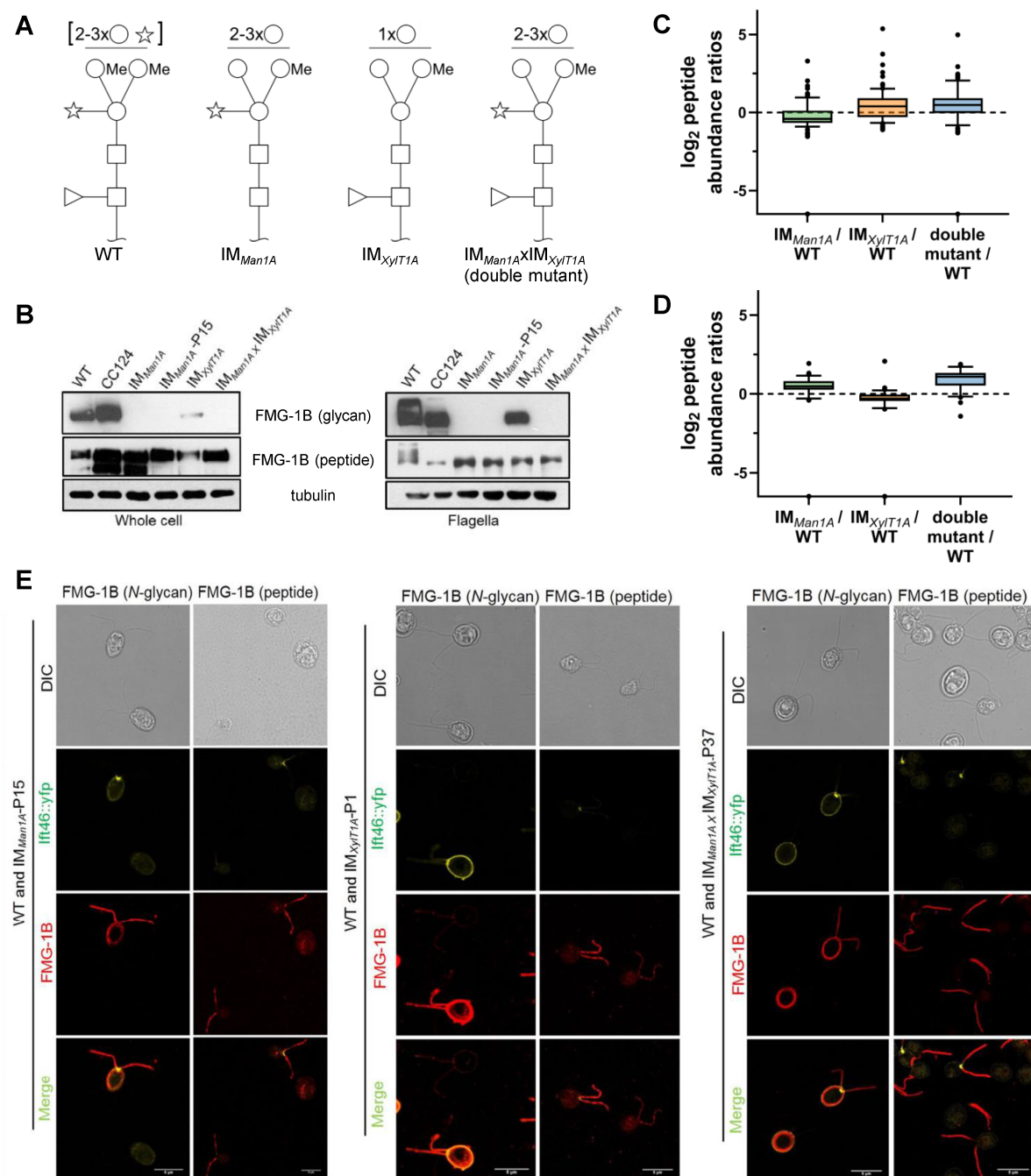183   considerably altered in the mutants versus WT.

Figure 1. Altered N-glycosylation of FMG-1B does not change its flagellar localization

A, Diagram of N-linked glycan compositions of mutant strains characterized in Schulze *et al.* 2018 and used in the current study. While IM$_{Man1A}$ and the double mutant are mainly characterized by a lower degree of methylation, N-glycans of IM$_{XylT1A}$ are decreased in length and lack the core xylose. All monosaccharides depicted above the horizontal line can be bound to any subjacent residue or to any residue at the same level. Square: N-Acetylglucosamine, Circe: hexose, Triangle: fucose, Star: xylose). B, Probing whole cell and flagella samples with antibodies directed against N-glycans or the protein backbone of FMG-1B.(Bloodgood et al., 1986) C, Log2

9

192   peptide abundances of FMG-1B obtained by label free MS analysis. D, Log2 peptide abundances of FAP-113

193   obtained by label free MS analysis. E, Immuno staining of WT-Ins (IFT46::YFP labelled) cells mixed with mutant

194   cells (IM$_{Man1A}$, IM$_{XylT1A}$ or IM$_{Man1A}$xIM$_{XylT1A}$) with antibodies of FMG-1B.

195   **Altered *N*-linked glycans attenuate bead attachment and movement to and along the**

196   **flagellar membrane**

197   In *C. reinhardtii,* polystyrene microspheres adhere to and move bidirectionally along the

198   flagellar surface.(Bloodgood, 1981) To check the effect of altered *N*-glycans on these processes,

199   beads with a diameter of 0.7 μm were added to cell suspensions of IM$_{Man1A}$, IM$_{XylT1A}$ and the

200   double mutant grown in M1 medium, and the number of beads attached to- or moved along

201   flagella were quantified (Fig. 2A and B). In WT-Ins strains, about 52 % of all flagella had at

202   least one bead attached, whereas the percentage of flagella with beads bound decreased to 46 %

203   in IM$_{Man1A}$, 33 % in IM$_{XylT1A}$ and 27 % in the double mutant (Fig. 2A). Among the beads

204   attached, 37 % moved along flagella of WT-Ins, 22 % in IM$_{Man1A}$, 29 % in IM$_{XylT1A}$ and 27 %

205   in the double mutant (Fig. 2B). These data suggested that interaction of flagellar membrane and

206   surface is altered due to altered *N*-glycan composition in these mutants.
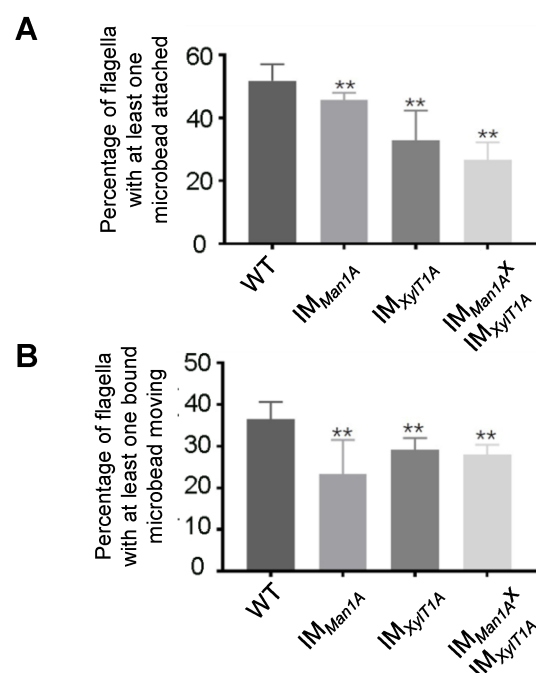
207

208

Figure 2. Altered *N*-glycosylation diminishes flagellar polystyrene bead attachment and -transport.

A, Percentage of flagella with at least one polystyrene bead bound. Cells were incubated with polystyrene beads (0.7 µm in diameter) and subsequently analyzed by light microscopy. B, Percentage of polystyrene beads transported along the flagellum with at least one polystyrene bead bound. Results present mean of three replicates with 50 cells analyzed per replicate. Error bars show SEM of three replicates. T-test was used for statistical analysis.

Quantification of the flagella mediated adhesion using atomic force microscopy

Flagella-mediated surface adhesion force was measured via atomic force microscopy (AFM) (Fig. 3A). Cells adhered to a cover slide were attached to an AFM cantilever via physical contact and unspecific binding (Liu et al., 2011). Subsequently, the AFM cantilever was pulled upwards and the force required to pull the cells off was recorded (Fig. 3B). To inhibit whole-cell gliding during AFM pulling, ciliobrevin D was used to inhibit dynein-1b activity and consequently the cell gliding ability (Firestone et al., 2012). Remarkably, the forces necessary to overcome the adhesion of *C. reinhardtii* flagella to the surface were significantly reduced in all IM strains analyzed as compared to WT-Ins (Fig. 3B and C). Especially in the double mutant

11

225 the average force was reduced from 8 nN in WT-Ins to 1 nN, while the average energy was

226 reduced from 4 to 0.5 J nm^{-1} (Fig. 3C and D). When dynein1-b inhibitor ciliobrevin D was

227 removed, the adhesion force of WT-Ins decreased from 8 nN to 3 nN, while this effect did not
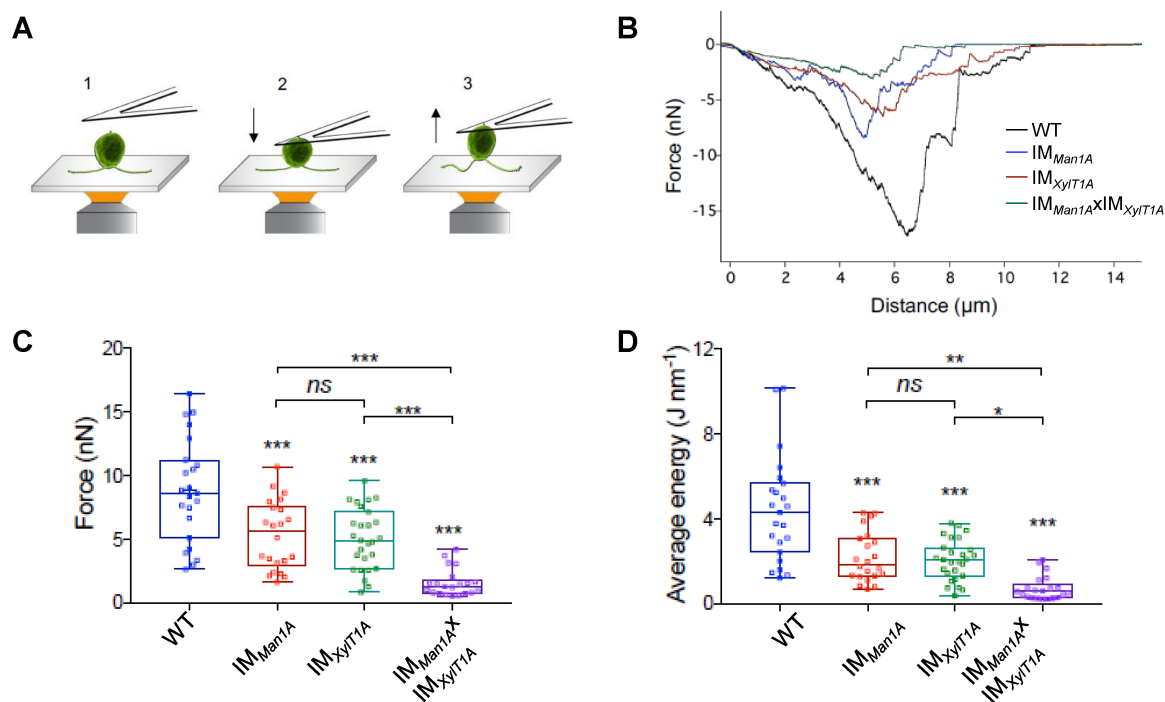
228 occur in the double mutant (Fig. 5A).

230 **Figure 3 Quantification of the flagella mediated adhesion using atomic force microscopy.**

231 A, Diagram of experimental procedures for force measurement: the cell adhered to the surface (1); the cell attached

232 to the AFM cantilever (2); the cell was pulled up from the surface by AFM cantilever (3). Please note, that

233 retrograde IFT, i.e. gliding was inhibited by ciliobrevin D during all measurements presented here. B,

234 Representative force curves acquired for strains including WT, IM$_{Man1A}$, IM$_{XylT1A}$ and IM$_{Man1A}$xIM$_{XylT1A}$. C, Flagella

235 adhesion forces of WT-Ins, IM$_{Man1A}$, IM$_{XylT1A}$ and IM$_{Man1A}$xIM$_{XylT1A}$ were generated from force curves (B). D,

236 Average energy of flagellar adhesion of WT-Ins, IM$_{Man1A}$, IM$_{XylT1A}$ and IM$_{Man1A}$xIM$_{XylT1A}$. Three biological

237 replicates were performed with minimum 5 cells measured per replicate. *p<0.05, **p<0.01, ***p<0.001. The p-

238 values are obtained from a two-sided, two sample t-test of mean values.

240 **Quantification of flagella adhesion using a micropipette force measurement approach**

12

241   To validate the AFM adhesion force measurements, an independent *in vivo* force measurement

242   approach(Backholm and Bäumchen, 2019; Kreis et al., 2018) was used with another genetic

243   background mutant, a xylosyltransferase 1A (CRISPR$_{XylT1A\_1}$) mutant, generated in parental

244   wildtype SAG11-32b (WT-SAG) by employing CRISPR/Cas9 (Figure 4 - Supplementary Fig.

245   1). As a wavelength dependency of flagellar adhesion had been revealed using this approach

246   (Backholm and Bäumchen, 2019), adhesion forces of the same cells were measured under

247   precisely controlled blue- and red-light conditions. Importantly, adhesion forces measured in

248   CRISPR$_{XylT1A\_1}$ were significantly diminished in comparison to respective WT-SAG, from

249   1.50 nN to 1.08 nN in blue light (Fig. 4A). Illuminating cells with red light dramatically

250   decreased the adhesion force in both WT-SAG and CRISPR$_{XylT1A\_1}$. Under red light, mean

251   adhesion forces of individual cells were dispersed broader in CRISPR$_{XylT1A\_1}$, yet, surface

252   adhesion was enhanced for CRISPR$_{XylT1A\_1}$ as compared to WT-SAG. In addition, micropipette

253   force measurements under blue light confirm that the presence of ciliobrevin D significantly

254   enhances the adhesiveness of the WT-SAG (Fig. 4B), while no significant effect of ciliobrevin

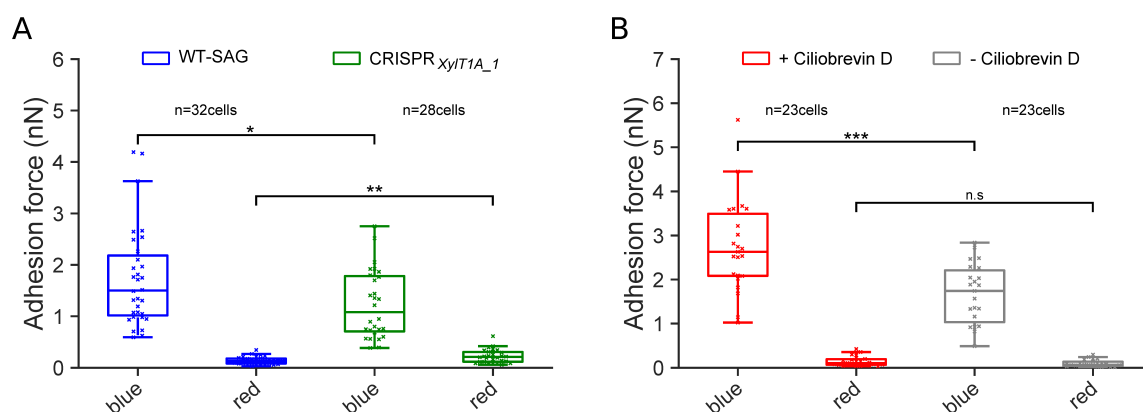255   D was observed in adhesion force measurements of the same cells in red light.

256

257

258

259 **Figure 4. Assessing flagella adhesion forces using micropipette force measurements**

260 A, Flagella mediated adhesion forces acquired for WT-SAG and a xylosyltransferase 1A mutant generated in the

261 genetic background of WT-SAG (CRISPR$_{XylT1A\_1}$). Micropipette force measurements of the same cells were

262 performed under blue and red light. B, Flagella mediated adhesion forces of WT-SAG in the absence (-) or presence

263 (+) of ciliobrevin D under blue and red light using the same technique. Mean values of 10 measurements per cell

264 are depicted, statistical analysis was performed on mean values: n.s: $p > 0.05$, $*p < 0.05$, $**p < 0.01$, $***p < 0.001$. The

265 p-values are obtained from Mann–Whitney U test.

266

267 **The effect of altered *N*-glycosylation on IFT and gliding**

268 The impact of ciliobrevin D on the adhesion force suggested that IFT might contribute to

269 surface adhesion forces. In addition, it implied that IFT might be hampered via altered *N*-

270 glycosylation. Therefore, IFT velocity and gliding ability of IFT46::YFP expressing WT-Ins

271 and IM$_{Man1A}$xIM$_{XylT1A}$ were assessed by using total internal reflection fluorescence (TIRF)

272 microscopy. Videos of adhered cells generated by TIRF microscopy were evaluated manually

273 via kymographs in ImageJ (Fig. 5B). Obtained data revealed that neither the proportion of non-

274 gliding events (gliding velocity smaller 0.3 $\mu m*s^{-1}$), nor gliding speed distribution was

275 significantly diminished when comparing WT-Ins and the double mutant (Fig. 5C). Likewise,

276 anterograde and retrograde IFT velocity was found at WT-Ins levels when comparing WT-Ins

277 and the double mutant (Fig. 5C), implying no significant impact of altered *N*-glycan maturation
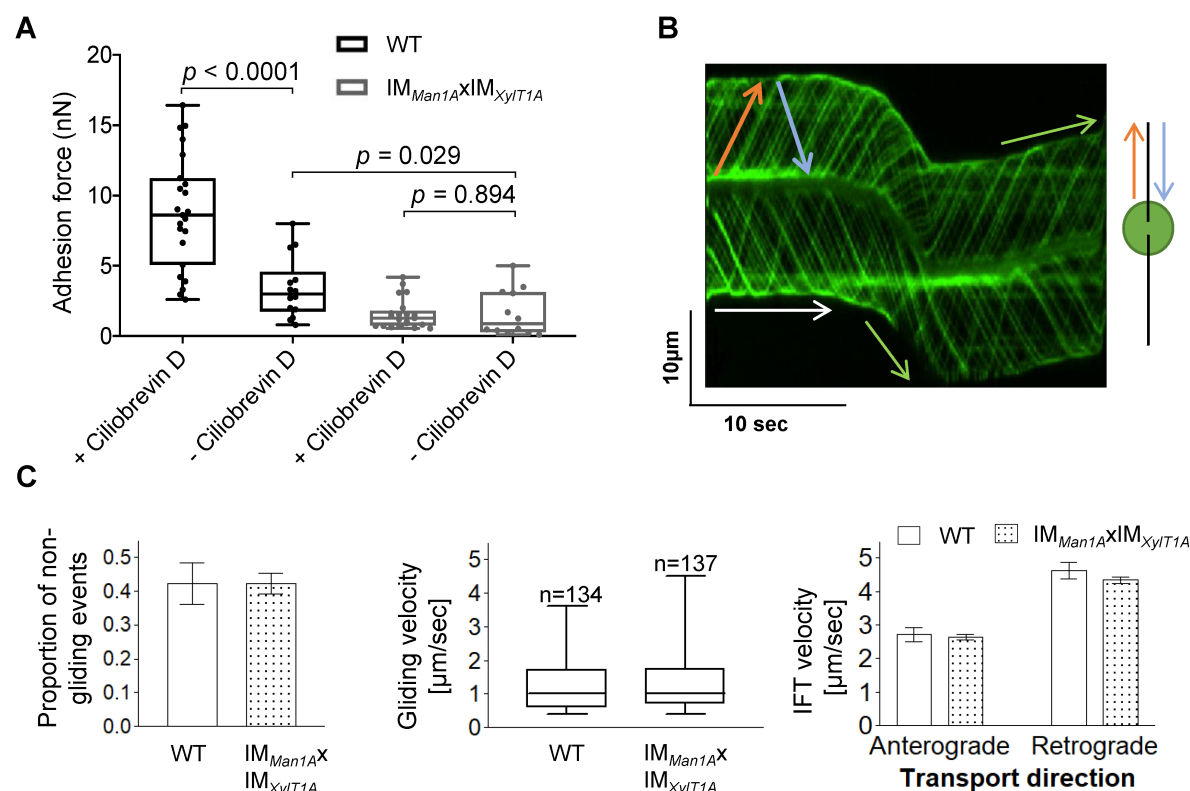
278 on IFT.

14

Figure 5. Ciliobrevin D enhances flagella mediated adhesion force in WT

A, Adhesion forces acquired for WT-Ins and the double mutant $IM_{Man1A}xIM_{XylT1A}$ in the absence or presence of ciliobrevin D, respectively. Three biological replicates were performed with minimum 5 cells measured per replicate. B, Representative kymograph of the movement of IFT46::YFP in flagella of WT-Ins acquired with TIRF microscopy used to calculate the velocity of gliding and IFT. White arrow: non-gliding event (v<0.3μm/s); green arrow: gliding event (v>0.3μm/s); red arrow: anterograde IFT track; blue: retrograde IFT track. C, IFT and gliding are not significantly altered in the double mutant compared to WT-Ins. Proportion of non-gliding events (left), gliding velocity (excluding non-gliding events; middle), IFT velocities in either direction (right). Three biological replicates were performed with 10 cells evaluated per replicate corresponding to 300 IFTs/replicate/strain in case of IFT velocity. Error bars in bar plots represent SD of three replicates. Student-t test was performed comparing mean values of replicates in regard of proportion of non-gliding events (p=0,415) and IFT-velocity (anterograde p= 0,284; retrograde p=0,065). Distribution of gliding velocities was analyzed by use of Mann-Whitney U test (p=0,421), n represents number of gliding events measured.

15

Discussion

Our data revealed that the maturation of *N*-glycans has an impact on flagella mediated cell adhesion in *C. reinhardtii.* At the same time, IFT and gliding velocity were not changed due to the altered *N*-glycosylation.

Microbead binding was found diminished in IM strains, implying that the flagellar surface has an altered affinity towards microbeads. In line with this, surface adhesion forces were significantly reduced compared to WT-Ins. The AFM data were confirmed by assessing another XylT1A mutant created via CRISPR/Cas9, using micropipette force measurements. It should be noted that *N*-glycan patterns of IM$_{XylT1A}$ and CRISPR$_{XylT1A}$ were comparable and thereby strengthen the proposed role of XylT1A as core xylosyltransferase (Lucas et al., 2020; Schulze et al., 2018). Forces measured for both WT strains in the absence of ciliobrevin D were similar in the approaches indicating the comparability of both methods, and confirmed that differential *N*-glycan maturation, i.e. altered *N*-glycan structures attached to mature proteins, lowers the adhesion force of flagella to a surface. These changes in adhesion forces were not accompanied by consistent drastic changes in the flagellar proteomes. For example, FMG-1B and FAP113, to date the only two known proteins involved in surface adhesion, were found in comparable amounts in WT-Ins and mutants (Fig. 1 and Figure 4 - Supplementary Fig. 2) (Bloodgood et al., 2019; Kamiya et al., 2018). Of note, also FMG-1A is localized in flagella and its amount was unaltered between WT and mutants in vegetative cells (Figure 1 - Supplementary Fig. 3). Interestingly, gliding of mutant strains on solid surface was not affected. The current model for flagella mediated cell adhesion and subsequent gliding proposes that the extracellular part of certain glycoproteins such as FMG-1B adheres to the surface, cytoplasmic moieties of these proteins are bound to ongoing retrograde IFT directly or indirectly upon calcium- and light dependent stimulus which is followed by an onset of gliding (Kreis et al., 2018; Shih et al., 2013). Assuming that altered *N*-glycan maturation does not impact initial protein folding in the

16

319   ER (as those steps are spatially and temporally separated), our data revealed that changed *N*-

320   glycosylation, did not alter targeting of respective glycoproteins to flagella nor the velocity of

321   IFT. Thus, changes in surface adhesion are likely linked to *N*-glycoprotein epitopes and their

322   direct interaction with the solid or semisolid surface.

323   Notably, ciliobrevin D enhanced adhesion forces measured for WT-Ins but not for the double

324   mutant. The difference may result from the activity of cytoplasmic dynein-1b, retrograde motor

325   of IFT. As IFT and gliding were not changed between double mutant and WT-Ins (Fig. 5), the

326   differential ciliobrevin D dependent adhesion forces imply that the ciliobrevin D mediated

327   enhancement of binding forces is not entirely due to IFT inhibition but more complex. Although

328   it is well accepted that ciliobrevin D specifically inhibits dynein-1b function, abolishes

329   retrograde IFT and is therefore widely used in cilia/flagella research, strikingly little is known

330   about its mode of action.(Firestone et al., 2012) When first described, it was suggested that it

331   would impair ATPase activity and not much knowledge was gained ever since (Roossien et al.,

332   2015). Clearly, more work is required to understand the mechanics of the ciliobrevin D-induced

333   enhancement of adhesion force (Fig.4 and 5).

334   The fact that the altered *N*-glycosylation diminished the force of cells to adhere to surfaces but

335   did not affect IFT, strongly suggests that adhesion to surfaces and IFT are not necessarily

336   coupled. As discussed below, adhesion probably evolved independently of the necessity to

337   enable cell gliding.

338   As described before, the adhesion forces for both strains were significantly stronger under blue

339   than under red light (Fig. 4A). Under blue light, the adhesion force for CRISPR*$_{XylT1A}$* was

340   significantly weaker compared to WT-SAG, consistent with what was observed via the AFM

341   force measurements (Fig. 3). Momentarily, there are no mechanistic insights regarding the light

342   dependence of *C. reinhardtii* adhesion and also the functional blue-light photoreceptor remains

17

343   to be identified. Yet, the red-light suppression of adhesion is diminished in CRISPR$_{XylT1A}$,

344   indicating that *N*-glycosylation might also impact flagellar driven processes other than

345   adhesion.

346   In summary, taking advantage of single-cell adhesion force measurements, our data revealed

347   that cell adhesion was significantly impaired in *C. reinhardtii N*-glycosylation mutant strains.

348   Our data further suggested that flagellar assembly, IFT and FMG-1B transport into flagella

349   were not affected by altered *N*-glycosylation. Thus, we conclude that proper *N*-glycosylation of

350   flagellar proteins is crucial for adhering *C. reinhardtii* cells onto surfaces. We further suggest

351   that the remaining adhesion force, although diminished in *N*-glycan mutants, is still sufficient

352   for gliding. This implies that the evolution of adhesion was not governed by the capability of

353   gliding but adhesion itself. Given the response of flagellar adhesion blue light, it could

354   potentially link adhesion to photo-protection which is also blue-light mediated, as blue light

355   mediated adhesion might result in photoprotection via cell shading (Kreis et al., 2018;

356   Petroutsos et al., 2016).

357

358

359   **Material and Methods**

360   **Culture growth**

361   Cells were grown photoheterotrophically in tris-acetate-phosphate (TAP) medium under

362   constant illumination at 50 µmol photons*s^{-1}*cm^{-2} unless stated otherwise.

363   **Measurement of flagellar length and flagellated cells**

364   The cells were fixed with 0.5% Lugol's solution for 1h at room temperature. Flagellar length

365   measurements were performed using a phase microscope (Nikon Eclipse Ti) equipped with an

366 electron multiplying charged-coupled device. For each sample, at least 50 flagella were

367 measured. For the measurement of flagellated cells, at least 100 cells were counted for each

368 strain in biological triplicates.

369 **Generation and analysis of a CRISPR/Cas9 mutant strain**

370 Mutagenesis was performed on the WT strain SAG11-32b following the protocol described in

371 Greiner *et al.* 2017 employing the transformation of a pre-built Cas9:guideRNA complex (Cas9

372 target sequence in the XylT1A gene: ACGAACACCCCAACACCAAT) simultaneously with

373 a plasmid encoding for a paromomycin resistance via electroporation. Following selection with

374 paromomycin, putative mutants were screened by PCR using the primer pairs short_fw:

375 TACAAAGAACGGGACGCAGG, short_rev: CATTGAAGCTCATCCAGACAC and

376 long_fw: AAGGGTCACGGCACGGTATG, long_rev: CCTGAAGCACCCATGATGCACG.

377 Genomic *XylT1A* regions of candidate strains showing not-WT like band patterns were

378 sequenced. In total, two mutant strains differing in the DNA inserted following the Cas9 cutting

379 site were identified (CRISPR$_{XylT1A\_1}$ and CRISPR$_{XylT1A\_2}$). Next, XylT1A protein levels were

380 quantified by parallel reaction monitoring (PRM) and supernatant *N*-glycan compositions were

381 assessed by IS-CID mass spectrometry. Additionally, flagella were isolated, separated by

382 SDS-PAGE and, after transferred to a nitrocellulose membrane, probed with the protein

383 backbone FMG-1B specific antibody.

384 **Flagella isolation**

385 Flagella isolation from cultures in the mid-log growth phase was performed as described

386 elsewhere by the pH shock method (Witman et al., 1972). Pellets containing flagella samples

387 were stored at -80°C until further use for immunoblotting or sample preparation for mass

388 spectrometric measurements.

19

Immunoblotting

390 Frozen, dry flagella and whole cell samples were resuspended in lysis buffer (10mM Tris/HCl,

391 pH=7.4, 2 % SDS, 1 mM Benzamidine and 1 mM PMSF) and subjected to sonication for

392 10 min. After pelleting the not-soluble cell debris, the protein concentration was determined

393 using the bicinchoninic acid assay (BCA Protein Assay Kit by Thermo Scientific Pierce).

394 Volumes corresponding to 30 µg of protein were separated by SDS-PAGE, transferred to

395 nitrocellulose membranes and incubated with antibodies as indicated.

Sample preparation for mass spectrometric measurements

397 Frozen, dry flagella and whole cell samples were treated as described in *Immunoblotting*.

398 Volumes corresponding to 60 µg of protein were tryptically digested and desalted as described

399 elsewhere (Rappsilber et al., 2007).

Mass spectrometry measurements

401 Tryptic peptides were reconstituted in 2 % (v/v) acetonitrile/0.1 % (v/v) formic acid in ultrapure

402 water and separated with an Ultimate 3000 RSLCnano System (Thermo Scientific).

403 Subsequently, the sample was loaded on a trap column (C18 PepMap 100, 300 µm x 5 mm,

404 5 mm particle size, 100 Å pore size; Thermo Scientific) and desalted for 5 min using 0.05 %

405 (v/v) TFA/2 % (v/v) acetonitrile in ultrapure water with a flow rate of 10 µL*min^{-1}. Following,

406 peptides were separated on a separation column (Acclaim PepMap100 C18, 75 mm i.D., 2 mm

407 particle size, 100 Å pore size; Thermo Scientific) with a length of 50 cm. General mass

408 spectrometric (MS) parameters are listed in Figure 1 - Supplementary Table 1.

409 For quantification of glycosyltransferases, PRM (including a target list) was employed on

410 whole cell samples and respective spectra were analyzed with the Skyline software (Pino et al.,

411 2017). For quantification of flagellar proteins, flagella samples were measured in biological

412 quadruplicates in standard, not targeted, data dependent measurements. Following, peptide wise

413   protein abundance ratios (IM/WT) were calculated with ProteomeDiscoverer™ (normalizing

414   on a set of not membrane standing flagellar proteins) and filtered for proteins identified in at

415   least 11 samples, for proteins having Abundance Ratio Adj. P-Value < 0.05 for at least one ratio

416   and for proteins appearing in the flagellar proteome ChlamyFPv5.(Pazour et al., 2005)

417   In order to assign glycopeptides, samples were measured employing In-Source collision

418   induced dissociation (IS-CID) as described previously followed by analysis of data with Ursgal

419   and SugarPy (Kremer et al., 2016; Oltmanns et al., 2020; Schulze et al., 2020).

420   **Microbead measurements**

421   Microbead binding- and transport assays were performed analogous to previous

422   descriptions.(Bloodgood et al., 2019) Monodisperse polystyrene microspheres (0.7 μm

423   diameter) were purchased from Polysciences, Inc. Beads were washed with deionized water for

424   three times and resuspended in NFHSM to make a store solution, which was used at 1:10

425   dilution in adhesion and motility detecting experiment.

426   To quantify the ability of bead binding, beads were added to 500 μL of cells at a density of

427   2×10^7 cells*mL^{-1}. After 5min, cells were observed with a light microscope (Olympus, U-

428   HGLGPS, 100X oil objective). A flagellum was scored as "+ bead" if beads adhered to it. The

429   percentage of flagellar binding beads was calculated as: Percentage of flagellar binding beads

430   = the number of "+ bead"/ (total number flagella scored) x 100%.

431   To obtain a kinetic measure of surface motility, cells were mixed with beads as above for 5 min

432   and randomly observed under the light microscope. Each bead adhered to a flagellum was

433   monitored for about 30 seconds. If beads moved along the flagella, we marked it as "Moved

434   bead" or it was "Adhered bead". The surface motility was calculated as: Percentage of moved

435   beads along with flagella= "Move bead" x/ ("Moved bead" + "Adhered bead") 100%.

AFM measurements

C. reinhardtii strains, grown in M1 medium under constant white illumination were grown for 65 h, were allowed to adhere to a glass slide (immersed in ethanol for overnight, subsequently rinsed with MQ water) in fresh M1 medium for 15 min. Following, cells were incubated in the presence of ciliobrevin D for 1 h (500 µL M1 supplemented with 200 µM ciliobrevin D). For AFM measurements, only adhered cells in gliding conformation having approximately similar appearance were analyzed. The MLCT-O10 AFM probe (Spring Const.: 0.03 N m^{-1}, length: 215 µm, width: 20 µm, resonant freq.: 15 kHz, Bruker) was soaked in acetone for 5 min, then subjected to UV illumination (distance to lamp: 3-5 mm) for 15 min. Then, the probe was immersed in 0.01 % poly-l-lysine for 1 h and afterwards rinsed with MQ water. Following, the probe was immersed with 2 % glutaraldehyde for 1 h and rinsed with MQ water before use. The AFM measurement was performed in Force Spectroscopy Mode in liquid at room temperature using a NanoWizard 3 AFM (JPK) equipped with a CellHesion stage (Z range: 100 µm) NanoWizard 3 head. The tip spring constant was routinely calibrated. The AFM tip, modified as described, was lowered onto the cell surface at a rate of 10 µm s^{-1} with a z scale of 25 µm. After contact, the applied force was maintained at 3 nN for 15 s. Then, the cell-attached probe was upraised at a rate of 1 µm s^{-1}. Force curves were processed with JPK SPM Data Processing (JPK). The forces and energy were determined as described in Figure 3 - Supplemental Figure 1 (Liu et al., 2011). Three biological replicates were performed with minimum 5 cells measured per replicate.

Micropipette force measurements

Culture growth and micropipette force measurements were performed following established recipes.(Kreis et al., 2019, 2018) In brief, *C. reinhardtii* strains WT-SAG and CRISPR$_{XylT1A\_1}$ were grown axenically in tris-acetate-phosphate (TAP) medium (Thermo Fisher Scientific) in a Memmert IPP 100Plus incubator on a 12h day / 12h night cycle. The experimental approach is

461 based on the use of a homemade micropipette force sensor, which allows for grasping a living

462 cell by suction (Backholm and Bäumchen, 2019). The adhesion force is obtained by bringing

463 the flagella into contact with a cleaned piece of a silicon wafer (Si-Mat, unilateral polished),

464 and by measuring the micropipette deflection during iterative approach and retraction of the

465 substrate. The illumination wavelength for blue and red light was 470 nm and 671 nm,

466 respectively, and realized by using narrow band pass interference filters (FWHM: 10 nm).

467 During the adhesion force measurements, the cells were illuminated with a constant photon flux

468 of 10^{19} photons m^{-2} s^{-1} for both light conditions. For each cell, 10 adhesion force measurements

469 were performed for each wavelength, whereby the order of red and blue light was varied

470 randomly after 5 consecutive measurements. For testing the influence of ciliobrevin D, a 200

471 µM solution of ciliobrevin D (Merck, Darmstadt, Germany) was prepared in a 9:1 water-

472 dimethylsulfoxid (DMSO, Sigma-Aldrich, Germany, Purity: 99.9%) mixture. *C. reinhardtii* cells were

473 incubated in the ciliobrevin D solution for 30 minutes. Since a high DMSO concentration in the TAP

474 medium causes death of the cells, the volume fraction of DMSO was kept at a level of about 3.6% during

475 the incubation and experiments. After the incubation, the culture was centrifuged at 100 *g* for ten minutes

476 to concentrate dead cells at the bottom of the incubation flask. The culture was then rested in the

477 incubator before the experiments for at least 30 minutes. At last, the upper part of the culture in the flask

478 was used to fill the liquid cell to perform the experiments. In parallel, a second sample of *C. reinhardtii*

479 cells was incubated with the same fraction of DMSO (without ciliobrevin D) and followed by the same

480 experimental procedure to serve as a control group.

481

482 **TIRF imaging**

483 Total internal reflection microscopy (TIRF) was applied to assess intraflagellar transport and

484 gliding behaviour of *C. reinhardtii* strains expressing YFP-coupled IFT46. Therefore, cell

485 densities were adjusted to $1*10^5$ cells*ml^{-1}. Samples were loaded to a glass bottom microscopy

486 chamber (µ-Slide 8 Well Glass Bottom) and refreshed every 20 min while imaging. TIRF

487 microscopy was performed at room temperature with a Nikon Eclipse Ti and a 100x objective.

488 IFT46::YFP was excited at 488 nm and fluorescence was recorded with an iXon Ultra EMCCD

489 camera (Andor). For analysis, images were captured with NIS-Elements software over 30 s at

490 10 fps and a pixel size of 0.158 μm*pixel^{-1}. Images were evaluated by use of Fiji via manual

491 evaluation of kymographs. Nett IFT velocities during gliding were calculated by subtracting

492 corresponding gliding velocities. Three biological replicates were performed with 10 cells in

493 gliding configuration analysed per replicate.

494 **Confocal Imaging**

495 Cells were incubated with primary antibodies (FMG-1B #8 and #61, available at dshb.com),

496 subsequently incubated with a fluorescently labeled secondary antibody and analyzed by

497 confocal microscopy as described previously (Lv et al., 2017). In brief, cells were plated on

498 1 % poly(ethyleneimine) coated cover glass, decolorized and fixed in methanol at -20 °C for

499 20 min, permeated cells in PBS buffer for 1 h, and then blocked in 5 % BSA (Biosharp), 10 %

500 normal goat serum (Dingguo) and 1 % fish gelatin (Sigma) in PBS. Incubated the samples with

501 primary antibodies overnight, washed them, and incubated secondary antibody, washed the

502 samples and mounted them on slides with nail polish.

503 **Acknowledgements**

24

511   Göttingen Algae Culture Collection (SAG) for providing the WT-SAG strain and R. Catalan

512   for technical assistance.

513   **Author contributions:**

514   N.X and L.H. performed light microscope imaging. A.O., J.B. and M.S. performed mass

515   spectrometry assisted data analysis. N.X., A.O. and J.B. performed immuno blotting

516   experiments. A.O. and S.K. performed CRISPR-Cas mutagenesis with help of P.H.. L.Z and

517   L.L performed AFM measurements and corresponding data interpretation. A.G., M.K. and O.B.

518   performed and analyzed micropipette force measurements. A.O., N.X., L.H., K.H. and M.H.

519   were involved in data interpretation. A.O. wrote the manuscript with help of N.X., L.H., M.H.

520   and K.H.

521   **Competing Interests:**

522   The authors declare no conflict of interests.

523   **Materials and Correspondence:**

524   The mass spectrometry proteomics data have been deposited to the ProteomeXchange

525   Consortium (http://proteomecentral.proteomexchange.org) via the PRIDE partner repository

526   with the dataset identifier PXD018353 and will be publically available upon acceptance of the

527   manuscript (Perez-Riverol et al., 2019). During peer review, the dataset can be entered via the

528   account reviewer44250@ebi.ac.uk and the password OLy6xQJY. For further requests, please

529   contact K. Huang (huangky@ihb.ac.cn) or M. Hippler (mhippler@uni-muenster.de).

530   **Literature cited**
531   Adams BM, Oster ME, Hebert DN. 2019. Protein Quality Control in the Endoplasmic
532   Reticulum. *Protein J* **38**:317–329. doi:10.1007/s10930-019-09831-w

533   Backholm M, Bäumchen O. 2019. Micropipette force sensors for in vivo force measurements
534   on single cells and multicellular microorganisms. *Nat Protoc* **14**:594–615.
535   doi:10.1038/s41596-018-0110-x

536 Bloodgood RA. 2009. The Chlamydomonas Flagellar Membrane and Its Dynamic Properties
537   In: Harris EH, Stern DB, Witman GB, editors. The Chlamydomonas Sourcebook.
538   London: Academic Press. pp. 309–368. doi:10.1016/B978-0-12-370873-1.00048-4

539 Bloodgood RA. 1987. Glycoprotein dynamics in the chlamydomonas flagellar membrane.
540   *Adv Mol Cell Biol* **1**:97–130. doi:10.1016/S1569-2558(08)60358-6

541 Bloodgood RA. 1981. Flagella-dependent gliding motility in Chlamydomonas. *Protoplasma*
542   **106**:183–192. doi:10.1007/BF01275550

543 Bloodgood RA, Salomonsky NL. 1998. Microsphere attachment induces glycoprotein
544   redistribution and transmembrane signaling in the Chlamydomonas flagellum.
545   *Protoplasma* **202**:76–83. doi:10.1007/BF01280876

546 Bloodgood RA, Tetreault J, Sloboda RD. 2019. The Chlamydomonas flagellar membrane
547   glycoprotein FMG-1B is necessary for expression of force at the flagellar surface. *J Cell*
548   *Sci* **132**:1–10. doi:10.1242/jcs.233429

549 Bloodgood RA, Woodward MP, Salomonsky NL. 1986. Redistribution and shedding of
550   flagellar membrane glycoproteins visualized using an anti-carbohydrate monoclonal
551   antibody and concanavalin A. *J Cell Biol* **102**:1797–1812. doi:10.1083/jcb.102.5.1797

552 Bloodgood RA, Workman LJ. 1984. A flagellar surface glycoprotein mediating cell-substrate
553   interaction in Chlamydomonas. *Cell Motil* **4**:77–87. doi:10.1002/cm.970040202

554 Cherepanova N, Shrimal S, Gilmore R. 2016. N-linked glycosylation and homeostasis of the
555   endoplasmic reticulum. *Curr Opin Cell Biol* **41**:57–65.
556   doi:doi:10.1016/j.ceb.2016.03.021

557 Cole DG, Diener DR, Himelblau AL, Beech PL, Fuster JC, Rosenbaum JL. 1998.
558   Chlamydomonas kinesin-II-dependent intraflagellar transport (IFT): IFT particles
559   contain proteins required for ciliary assembly in Caenorhabditis elegans sensory neurons.
560   *J Cell Biol* **141**:993–1008. doi:10.1083/jcb.141.4.993

561 Collingridge P, Brownlee C, Wheeler GL. 2013. Compartmentalized calcium signaling in
562   cilia regulates intraflagellar transport. *Curr Biol* **23**:2311–2318.
563   doi:10.1016/j.cub.2013.09.059

564 Firestone AJ, Weinger JS, Maldonado M, Barlan K, Langston LD, O'Donnell M, Gelfand VI,
565   Kapoor TM, Chen JK. 2012. Small-molecule inhibitors of the AAA+ ATPase motor
566   cytoplasmic dynein. *Nature* **484**:125–129. doi:10.1038/nature10936

567 Gardner BM, Pincus D, Gotthardt K, Gallagher CM, Walter P. 2013. Endoplasmic reticulum
568   stress sensing in the unfolded protein response. *Cold Spring Harb Perspect Biol* **5**:1–15.
569   doi:10.1101/cshperspect.a013169

570 Huangfu D, Liu A, Rakeman AS, Murcia NS, Niswander L, Anderson K V. 2003. Hedgehog
571   signalling in the mouse requires intraflagellar transport proteins. *Nature* **426**:83–87.
572   doi:10.1038/nature02061

573 Ishikawa H, Marshall WF. 2011. Ciliogenesis: Building the cell's antenna. *Nat Rev Mol Cell*
574   *Biol* **12**:222–234. doi:10.1038/nrm3085

575 Kamiya R, Shiba K, Inaba K, Kato-Minoura T. 2018. Release of Sticky Glycoproteins from

576   Chlamydomonas Flagella During Microsphere Translocation on the Surface Membrane.
577   *Zoolog Sci* **35**:299. doi:10.2108/zs180025

578   Kaulfürst-Soboll H, Rips S, Koiwa H, Kajiura H, Fujiyama K, Von Schaewen A. 2011.
579   Reduced immunogenicity of Arabidopsis hgl1 mutant N-glycans caused by altered
580   accessibility of xylose and core fucose epitopes. *J Biol Chem* **286**:22955–22964.
581   doi:10.1074/jbc.M110.196097

582   Kozminski KG, Beech PL, Rosenbaum JL. 1995. The Chlamydomonas kinesin-like protein
583   FLA10 is involved in motility associated with the flagellar membrane. *J Cell Biol*
584   **131**:1517–1527. doi:10.1083/jcb.131.6.1517

585   Kozminski KG, Johnson KA, Forscher P, Rosenbaum JL. 1993. A motility in the eukaryotic
586   flagellum unrelated to flagellar beating. *Proc Natl Acad Sci* **90**:5519 LP – 5523.
587   doi:10.1073/pnas.90.12.5519

588   Kreis CT, Grangier A, Bäumchen O. 2019. In vivo adhesion force measurements of
589   Chlamydomonas on model substrates. *Soft Matter* **15**:3027–3035.
590   doi:10.1039/c8sm02236d

591   Kreis CT, Le Blay M, Linne C, Makowski MM, Bäumchen O. 2018. Adhesion of
592   Chlamydomonas microalgae to surfaces is switchable by light. *Nat Phys* **14**:45–49.
593   doi:10.1038/NPHYS4258

594   Kremer LPM, Leufken J, Oyunchimeg P, Schulze S, Fufezan C. 2016. Ursgal, Universal
595   Python Module Combining Common Bottom-Up Proteomics Tools for Large-Scale
596   Analysis. *J Proteome Res* **15**:788–794. doi:10.1021/acs.jproteome.5b00860

597   Kukuruzinska MA, Bergh MLE, Jackson BJ. 1987. Protein glycosylation in yeast. *Antonie*
598   *Van Leeuwenhoek* **56**:915–44. doi:10.1146/annurev.bi.56.070187.004411

599   Laib JA, Marin JA, Bloodgood RA, Guilford WH. 2009. The reciprocal coordination and
600   mechanics of molecular motors in living cells. *Proc Natl Acad Sci* **106**:3190 LP – 3195.
601   doi:10.1073/pnas.0809849106

602   Lechtreck KF. 2015. IFT-Cargo Interactions and Protein Transport in Cilia. *Trends Biochem*
603   *Sci* **40**:765–778. doi:10.1016/j.tibs.2015.09.003

604   Liu L-N, Duquesne K, Oesterhelt F, Sturgis JN, Scheuring S. 2011. Forces guiding assembly
605   of light-harvesting complex 2 in native membranes. *Proc Natl Acad Sci* **108**:9455 LP –
606   9459. doi:10.1073/pnas.1004205108

607   Long H, Zhang F, Xu N, Liu G, Diener DR, Rosenbaum JL, Huang K. 2016. Comparative
608   Analysis of Ciliary Membranes and Ectosomes. *Curr Biol* **26**:3327–3335.
609   doi:10.1016/j.cub.2016.09.055

610   Lucas P-L, Mathieu-Rivet E, Chan Tchi Song P, Oltmanns A, Loutelier-Bourhis C, Plasson
611   C, Afonso C, Hippler M, Lerouge P, Mati-Baouche N, Bardor M. 2020. Multiple
612   xylosyltransferases heterogeneously xylosylate protein N -linked glycans in
613   Chlamydomonas reinhardtii. *Plant J* **102**:230–245. doi:10.1111/tpj.14620

614   Lv B, Wan L, Taschner M, Cheng X, Lorentzen E, Huang K. 2017. Intraflagellar transport
615   protein IFT52 recruits IFT46 to the basal body and flagella. *J Cell Sci* **130**:1662–1674.

616   doi:10.1242/jcs.200758

617   Mathieu-Rivet E, Scholz M, Arias C, Dardelle F, Schulze S, Le Mauff F, Teo G, Hochmal
618   AK, Blanco-Rivero A, Loutelier-Bourhis C, Kiefer-Meyer MC, Fufezan C, Burel C,
619   Lerouge P, Martinez F, Bardor M, Hippler M. 2013. Exploring the N-glycosylation
620   pathway in chlamydomonas reinhardtii unravels novel complex structures. *Mol Cell*
621   *Proteomics* **12**:3160–3183. doi:10.1074/mcp.M113.028191

622   Oltmanns A, Hoepfner L, Scholz M, Zinzius K, Schulze S, Hippler M. 2020. Novel Insights
623   Into N-Glycan Fucosylation and Core Xylosylation in C. reinhardtii. *Front Plant Sci* **10**.
624   doi:10.3389/fpls.2019.01686

625   Pazour GJ, Agrin N, Leszyk J, Witman GB. 2005. Proteomic analysis of a eukaryotic cilium.
626   *J Cell Biol* **170**:103–113. doi:10.1083/jcb.200504008

627   Pedersen LB, Rosenbaum JLBT-CT in DB. 2008. Chapter Two Intraflagellar Transport (IFT):
628   Role in Ciliary Assembly, Resorption and SignallingCiliary Function in Mammalian
629   Development. Academic Press. pp. 23–61. doi:https://doi.org/10.1016/S0070-
630   2153(08)00802-8

631   Perez-Riverol Y, Csordas A, Bai J, Bernal-Llinares M, Hewapathirana S, Kundu DJ, Inuganti
632   A, Griss J, Mayer G, Eisenacher M, Pérez E, Uszkoreit J, Pfeuffer J, Sachsenberg T,
633   Yılmaz Ş, Tiwary S, Cox J, Audain E, Walzer M, Jarnuczak AF, Ternent T, Brazma A,
634   Vizcaíno JA. 2019. The PRIDE database and related tools and resources in 2019:
635   improving support for quantification data. *Nucleic Acids Res* **47**:D442–D450.
636   doi:10.1093/nar/gky1106

637   Petroutsos D, Tokutsu R, Maruyama S, Flori S, Greiner A, Magneschi L, Cusant L, Kottke T,
638   Mittag M, Hegemann P, Finazzi G, Minagawa J. 2016. A blue-light photoreceptor
639   mediates the feedback regulation of photosynthesis. *Nature* **537**:563–566.
640   doi:10.1038/nature19358

641   Pino LK, Searle BC, Bollinger JG, Nunn B, MacLean B, MacCoss MJ. 2017. The Skyline
642   ecosystem: Informatics for quantitative mass spectrometry proteomics. *Mass Spectrom*
643   *Rev* **n/a**. doi:10.1002/mas.21540

644   Porter ME, Bower R, Knott JA, Byrd P, Dentler W. 1999. Cytoplasmic Dynein Heavy Chain
645   1b Is Required for Flagellar Assembly in Chlamydomonas. *Mol Biol Cell* **10**:693–712.
646   doi:10.1091/mbc.10.3.693

647   Rappsilber J, Mann M, Ishihama Y. 2007. Protocol for micro-purification, enrichment, pre-
648   fractionation and storage of peptides for proteomics using StageTips. *Nat Protoc*
649   **2**:1896–1906. doi:10.1038/nprot.2007.261

650   Roossien DH, Miller KE, Gallo G. 2015. Ciliobrevins as tools for studying dynein motor
651   function. *Front Cell Neurosci* **9**:1–10. doi:10.3389/fncel.2015.00252

652   Rosenbaum JL, Witman GB. 2002. Intraflagellar transport. *Nat Rev Mol Cell Biol* **3**:813–825.
653   doi:10.1038/nrm952

654   Schulze S, Oltmanns A, Fufezan C, Krägenbring J, Pohlschröder M, Hippler M. 2020.
655   SugarPy facilitates the universal, discovery-driven analysis of intact glycopeptides.
656   *under Rev*.

657 Schulze S, Oltmanns A, Machnik N, Liu G, Xu N, Jarmatz N, Scholz M, Sugimoto K,
658   Fufezan C, Huang K, Hippler M. 2018. N-Glycoproteomic characterization of
659   mannosidase and xylosyltransferase mutant strains of chlamydomonas reinhardtii. *Plant*
660   *Physiol* **176**:1952–1964. doi:10.1104/pp.17.01450

661 Shih SM, Engel BD, Kocabas F, Bilyard T, Gennerich A, Marshall WF, Yildiz A. 2013.
662   Intraflagellar transport drives flagellar surface motility. *Elife* **2013**:1–19.
663   doi:10.7554/eLife.00744

664 Snell WJ, Pan J, Wang Q. 2004. Cilia and Flagella Revealed: From Flagellar Assembly in
665   Chlamydomonas to Human Obesity Disorders. *Cell* **117**:693–697.
666   doi:10.1016/j.cell.2004.05.019

667 Stanley P, Taniguchi N AM. 2017. N-glycans In: Varki A, editor. Essentials of Glycobiology.
668   Cold Spring Harbor (NY): Cold Spring Harbor Laboratory Press. pp. 99–111.
669   doi:10.1101/glycobiology.3e.009

670 Strasser R. 2016. Plant protein glycosylation. *Glycobiology* **26**:926–939.
671   doi:10.1093/glycob/cww023

672 Witman GB, Carlson K, Berliner J, Rosenbaum JL. 1972. Chlamydomonas flagella: I.
673   isolation and electrophoretic analysis of microtubules, matrix, membranes, and
674   mastigonemes. *J Cell Biol* **54**:507–539. doi:10.1083/jcb.54.3.507

675 Wood CR, Huang K, Diener DR, Rosenbaum JL. 2013. The cilium secretes bioactive
676   ectosomes. *Curr Biol* **23**:906–911. doi:10.1016/j.cub.2013.04.019

677

Supplementary Material corresponding to the publication

Altered *N*-glycan composition impacts flagella mediated adhesion in *Chlamydomonas reinhardtii*

Authored by:

N. Xu, A. Oltmanns, L. Zhao, A. Girot, M. Karimi, L. Hoepfner, S. Keltenborn, M. Scholz, J. Beißel, P. Hegemann, O. Bäumchen, L.N. Liu, K. Huang, M. Hippler

Table of content

Figure 1 - Supplementary Table 1. MS parameters. Relevant parameters used to acquire IS-CID and not fragmented TopN MS spectra as well as PRM data.

	TopN without IS-CID	In-Source CID HCD	Parallel reaction monitoring	
Eluent compositions	Peptide trapping: 0.05% trifluoroacetic acid (TFA) in ultrapure water (A1), 0.05% TFA in 80% acetonitrile (B1) Peptide separation: 0.1% formic acid (FA) in ultrapure water (A2), 0.1% FA in 80% acetonitrile (B2)			LC parameters
Trap Column	C18 PepMap 100, 300 µM x 5 mm, 5 µm particle size, 100 Å pore size; Thermo Scientific			
Peptide trapping (eluents A1+B1)	2.5% B1 at 5 µl/min for 5 min	2.5% B1 at 10 µl/min for 3 min		
Flow rate	300 nL/min	250 nL/min		
Separation Column	Acclaim PepMap C18, 75 µm x 50 cm, 2 µm particle size, 100 Å pore size; Thermo Scientific			
Gradient for peptide separation (eluents A2+B2)	2.5% B2 over 5 min, 2.5-45% B2 over 40 min, 45%-99 % B2 over 5 min 99% B2 for 20 min 99%-2.5% over 5 min 2.5% for 30 min	2.5% B2 over 5 min, 2.5-35% B2 over 105 min, 35%-99 % B2 over 5 min 99% B2 for 20 min 99%-2.5% over 5 min 2.5% for 40 min		
In-source CID	off	80 eV	off	
Use lock masses	off		on (m/z 445.12003)	MS1 settings
Resolution at *m/z* 200 (FWHM)	70,000			
Chromatographic peak width	15 s			
AGC target	3e6			
Maximum injection time	100 ms		50 ms	

Scan range	600-3000 m/z		350-1600 m/z	
Mass tags	off	on	off	
TopN	12		n/a	
Resolution at *m/z* 200 (FWHM)	17,500		35,000	
Isolation window	2 m/z		2 m/z (offset 0.5 m/z)	
AGC target	1e5			
Maximum injection time	120 ms			
Normalized collision energy (NCE)	30		27	
Minimum AGC target	1.25e3		n/a	
Intensity threshold	1e4		n/a	
Charge exclusion	unassigned, >5		n/a	
Dynamic exclusion	15 s		n/a	

(rightmost column label, rotated) **MS2 settings**
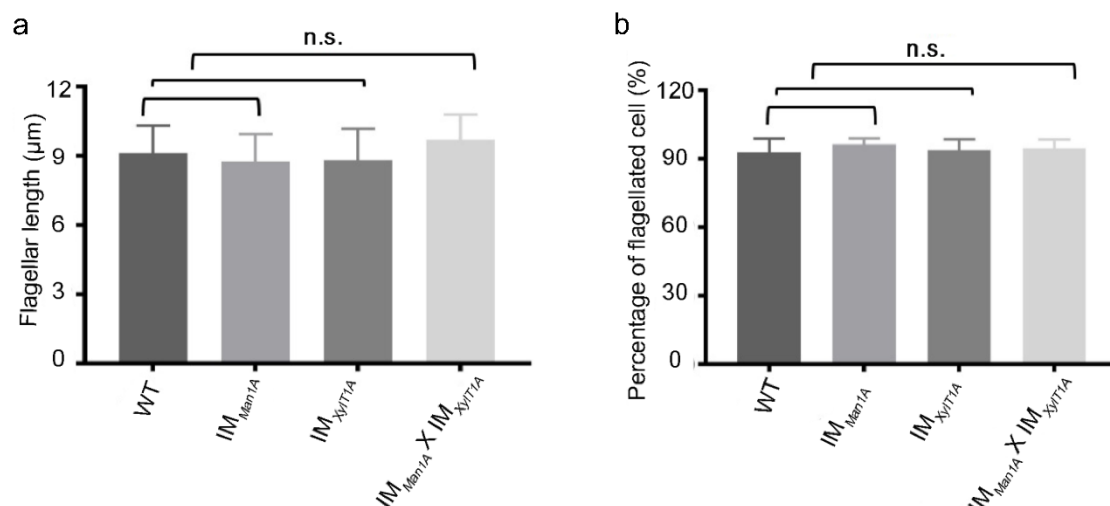
Figure 1 - Supplementary Figure 1. Flagellar length is not altered in *N*-glycosylation mutants.

a, Measurement of the flagellar length (in µm) among WT-Ins and three mutants. 50 flagella were measured in each experiment and this experiment has three biological repeats. Error bar: mean ± SD. p>0.05. b, Percentage of flagellated cell in WT-Ins and IM strains. The result of three biological replicates is showns. Error bar: mean ± SD. p>0.05.
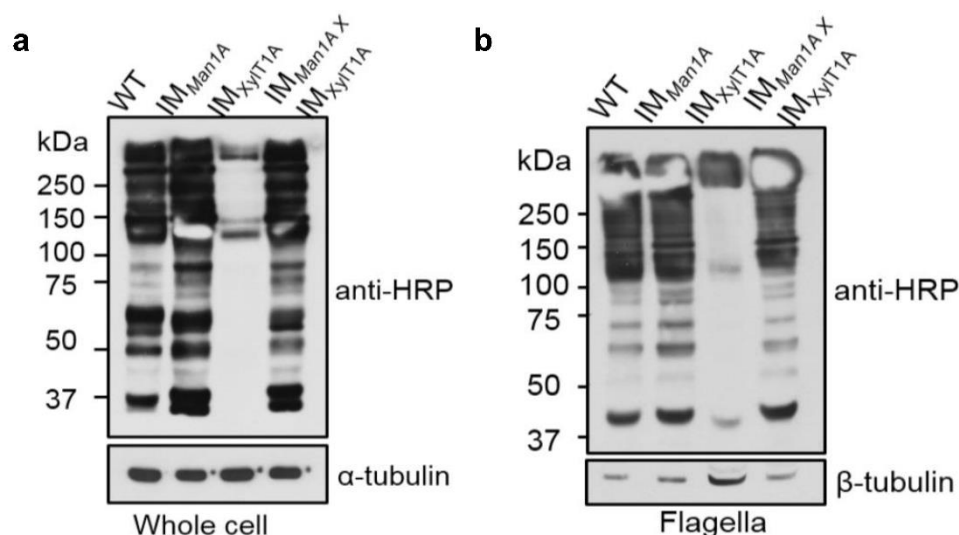
Figure 1 - Supplementary Figure 2. *N*-Glycan structures are altered in mutants as compared to WT-Ins.

Whole cell proteins (a) and isolated flagella (b) of WT-Ins and mutants were separated on a 7% SDS-PAGE, transferred to nitrocellulose and probed with anti-HRP, which is specifically binding to β1,2-xylose and α1,3-fucose attached to the *N*-glycan core. α-tubulin, as loading controls.
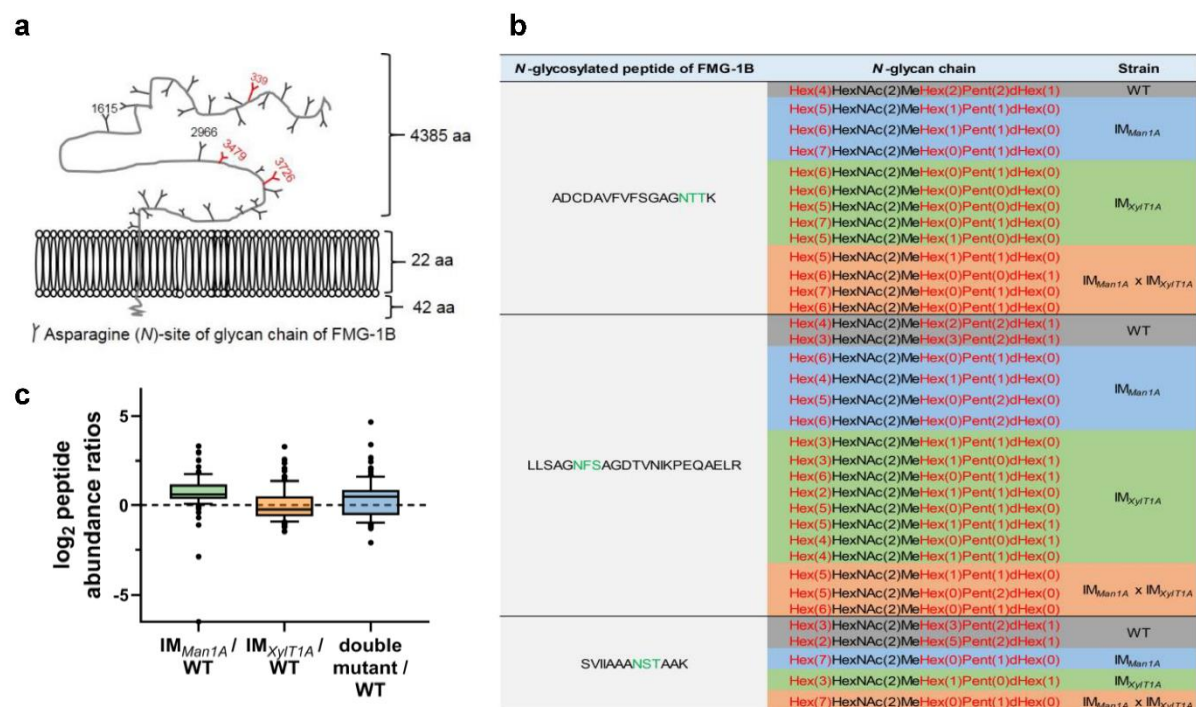
Figure 1 - Supplementary Figure 3. Change of *N*-glycan pattern of FMG-1B in IM strains as compared to WT-Ins.

a, Diagram of the topology of FMG-1B, the major component of the glycocalyx in *C. reinhardtii*. The identified *N*-linked glycosylation sites are marked. b, Comparison of FMG-1B proteotypic *N*-glycopeptides identified by IS-CID/SugarPy in WT-Ins, IM$_{Man1A}$, IM$_{XylT1A}$ and IM$_{Man1A}$xIM$_{XylT1A}$. c, The relative peptide abundances of FMG-1A in IM$_{Man1A}$, IM$_{XylT1A}$ and IM$_{Man1A}$xIM$_{XylT1A}$ strains compared it in WT-Ins obtained by label free MS analysis.
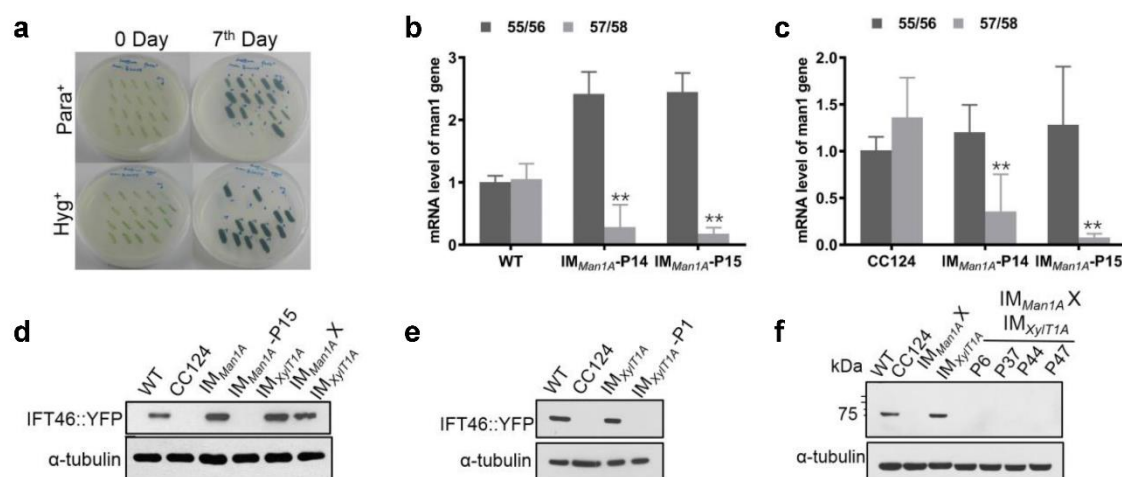
Figure 1 - Supplementary Figure 4. Genetic crossing of original IM strains (mt+) with CC124 (mt-) to obtain mutants lacking IFT46::YFP.

a, Screening the progenies of IM_{Man1A} mutants with WT-CC-124 to obtain the mutant without IFT46::YFP background, which grew in TAP plate with Paromomycin added and died in TAP plate with Hygromycin added. b, Determination of mRNA levels of *MAN1A* gene in progeny clones P14, P15 and WT-Ins. IM_{Man1A}-P14 still can live in TAP plate with Paromomycin or Hygromycin. IM_{Man1A}-P15 grew in TAP plate with Paromomycin and died in TAP plate added Hygromycin, which is the strain IFT46::YFP had been removed . Error bar: mean ± SD. Asterisks indicate statistically significant differences ($p < 0.01$). c, Comparison of mRNA level of *MAN1A* gene in progeny clones with CC-124. Error bar: mean+/- SD. Asterisks indicate statistically significant differences ($p < 0.01$). d, Determination of the expression of IFT46::YFP in whole cell of WT-Ins and IM_{Man1A}-P15 mutant. IM_{Man1A}-P15 is the offspring generated by crossing IM_{Man1A}-P15 mutant (mt+) with CC124 (mt-). α-tubulin, as loading control. e, Determination of the expression of IFT46::YFP in whole cell of WT-Ins and IM_{XylT1A}-P1 mutant. α-tubulin, as loading control. f, Determination of the expression of IFT46::YFP in progenies from the crossing CC124 with IM_{Man1A} X IM_{XylT1A}. α-tubulin, as loading control.

a, **b,**

c,

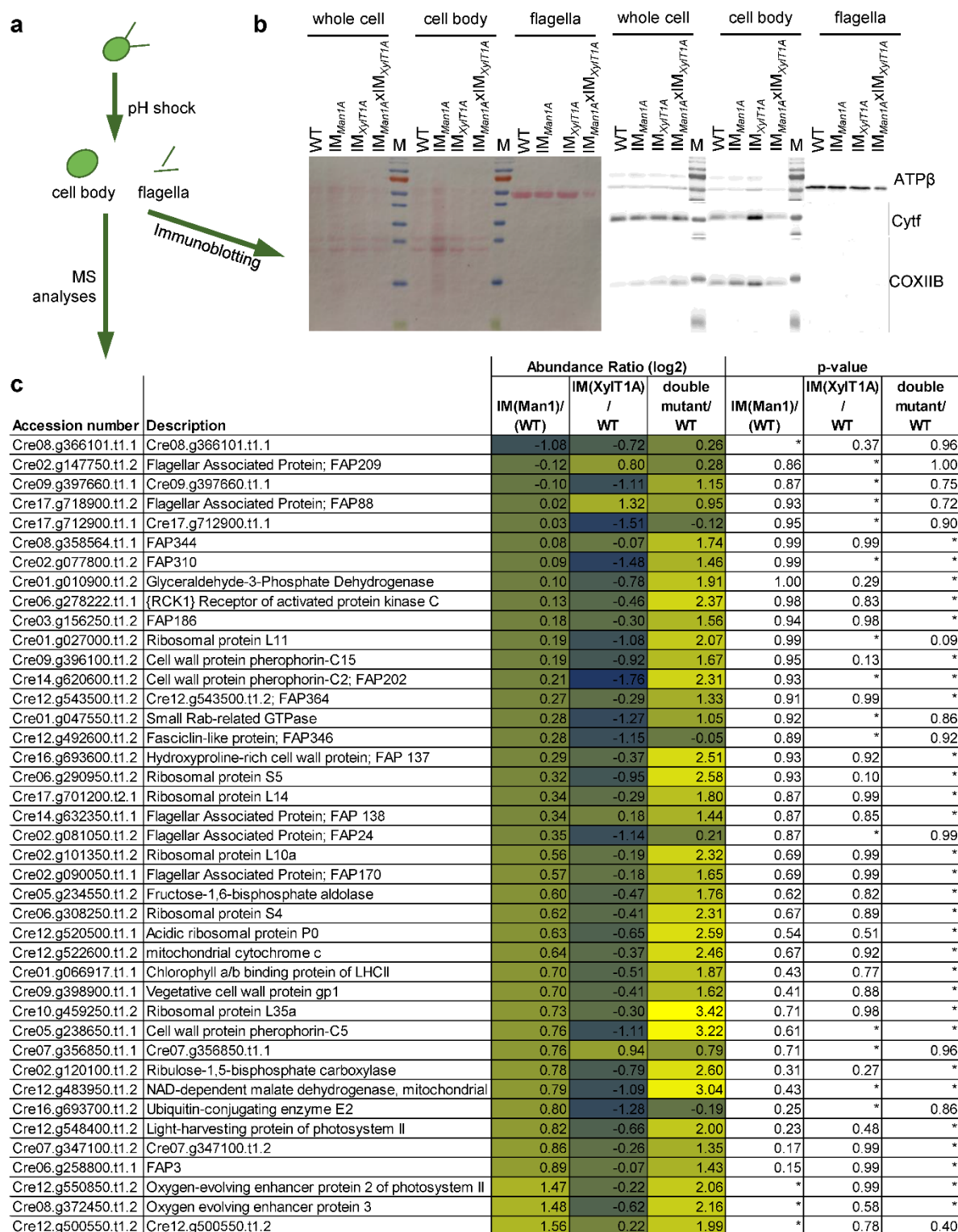| Accession number	Description	Abundance Ratio (log2)			p-value		
		IM(Man1)/ (WT)	IM(XylT1A)/ WT	double mutant/ WT	IM(Man1)/ (WT)	IM(XylT1A)/ WT	double mutant/ WT
Cre08.g366101.t1.1	Cre08.g366101.t1.1	-1.08	-0.72	0.26	*	0.37	0.96
Cre02.g147750.t1.2	Flagellar Associated Protein; FAP209	-0.12	0.80	0.28	0.86	*	1.00
Cre09.g397660.t1.1	Cre09.g397660.t1.1	-0.10	-1.11	1.15	0.87	*	0.75
Cre17.g718900.t1.1	Flagellar Associated Protein; FAP88	0.02	1.32	0.95	0.93	*	0.72
Cre17.g712900.t1.1	Cre17.g712900.t1.1	0.03	-1.51	-0.12	0.95	*	0.90
Cre08.g358564.t1.1	FAP344	0.08	-0.07	1.74	0.99	0.99	*
Cre02.g077800.t1.2	FAP310	0.09	-1.48	1.46	0.99	*	*
Cre01.g010900.t1.2	Glyceraldehyde-3-Phosphate Dehydrogenase	0.10	-0.78	1.91	1.00	0.29	*
Cre06.g278222.t1.1	{RCK1} Receptor of activated protein kinase C	0.13	-0.46	2.37	0.98	0.83	*
Cre03.g156250.t1.2	FAP186	0.18	-0.30	1.56	0.94	0.98	*
Cre01.g027000.t1.2	Ribosomal protein L11	0.19	-1.08	2.07	0.99	*	0.09
Cre09.g396100.t1.2	Cell wall protein pherophorin-C15	0.19	-0.92	1.67	0.95	0.13	*
Cre14.g620600.t1.2	Cell wall protein pherophorin-C2; FAP202	0.21	-1.76	2.31	0.93	*	*
Cre12.g543500.t1.2	Cre12.g543500.t1.2; FAP364	0.27	-0.29	1.33	0.91	0.99	*
Cre01.g047550.t1.2	Small Rab-related GTPase	0.28	-1.27	1.05	0.92	*	0.86
Cre12.g492600.t1.2	Fasciclin-like protein; FAP346	0.28	-1.15	-0.05	0.89	*	0.92
Cre16.g693600.t1.2	Hydroxyproline-rich cell wall protein; FAP 137	0.29	-0.37	2.51	0.93	0.92	*
Cre06.g290950.t1.2	Ribosomal protein S5	0.32	-0.95	2.58	0.93	0.10	*
Cre17.g701200.t2.1	Ribosomal protein L14	0.34	-0.29	1.80	0.87	0.99	*
Cre14.g632350.t1.1	Flagellar Associated Protein; FAP 138	0.34	0.18	1.44	0.87	0.85	*
Cre02.g081050.t1.2	Flagellar Associated Protein; FAP24	0.35	-1.14	0.21	0.87	*	0.99
Cre02.g101350.t1.2	Ribosomal protein L10a	0.56	-0.19	2.32	0.69	0.99	*
Cre02.g090050.t1.1	Flagellar Associated Protein; FAP170	0.57	-0.18	1.65	0.69	0.99	*
Cre05.g234550.t1.2	Fructose-1,6-bisphosphate aldolase	0.60	-0.47	1.76	0.62	0.82	*
Cre06.g308250.t1.2	Ribosomal protein S4	0.62	-0.41	2.31	0.67	0.89	*
Cre12.g520500.t1.1	Acidic ribosomal protein P0	0.63	-0.65	2.59	0.54	0.51	*
Cre12.g522600.t1.2	mitochondrial cytochrome c	0.64	-0.37	2.46	0.67	0.92	*
Cre01.g066917.t1.1	Chlorophyll a/b binding protein of LHCII	0.70	-0.51	1.87	0.43	0.77	*
Cre09.g398900.t1.1	Vegetative cell wall protein gp1	0.70	-0.41	1.62	0.41	0.88	*
Cre10.g459250.t1.2	Ribosomal protein L35a	0.73	-0.30	3.42	0.71	0.98	*
Cre05.g238650.t1.1	Cell wall protein pherophorin-C5	0.76	-1.11	3.22	0.61	*	*
Cre07.g356850.t1.1	Cre07.g356850.t1.1	0.76	0.94	0.79	0.71	*	0.96
Cre02.g120100.t1.2	Ribulose-1,5-bisphosphate carboxylase	0.78	-0.79	2.60	0.31	0.27	*
Cre12.g483950.t1.2	NAD-dependent malate dehydrogenase, mitochondrial	0.79	-1.09	3.04	0.43	*	*
Cre16.g693700.t1.2	Ubiquitin-conjugating enzyme E2	0.80	-1.28	-0.19	0.25	*	0.86
Cre12.g548400.t1.2	Light-harvesting protein of photosystem II	0.82	-0.66	2.00	0.23	0.48	*
Cre07.g347100.t1.2	Cre07.g347100.t1.2	0.86	-0.26	1.35	0.17	0.99	*
Cre06.g258800.t1.1	FAP3	0.89	-0.07	1.43	0.15	0.99	*
Cre12.g550850.t1.2	Oxygen-evolving enhancer protein 2 of photosystem II	1.47	-0.22	2.06	*	0.99	*
Cre08.g372450.t1.2	Oxygen evolving enhancer protein 3	1.48	-0.62	2.16	*	0.58	*
Cre12.g500550.t1.2	Cre12.g500550.t1.2	1.56	0.22	1.99	*	0.78	0.40

Figure 1 - Supplementary Figure 5. Quantitative mass spectrometry of isolated flagellar from WT-Ins and *N*-glycosylation mutants

a, Experimental procedures of flagella isolation and following analyses. b, Immunoblot of isolated flagella probed with antibodies against chloroplast marker protein (Cytf, cytochrome f) and mitochondrium marker protein (COXIIB). The absence of respective marker proteins in the flagellar fraction prove the purity of flagellar samples while ponceau staining of the same membrane indicates that similar amounts of protein were loaded. c, Proteins found significantly differential in abundance in IM strains compared to WT-Ins. Entries of proteins are given with corresponding phytozome ID protein description.
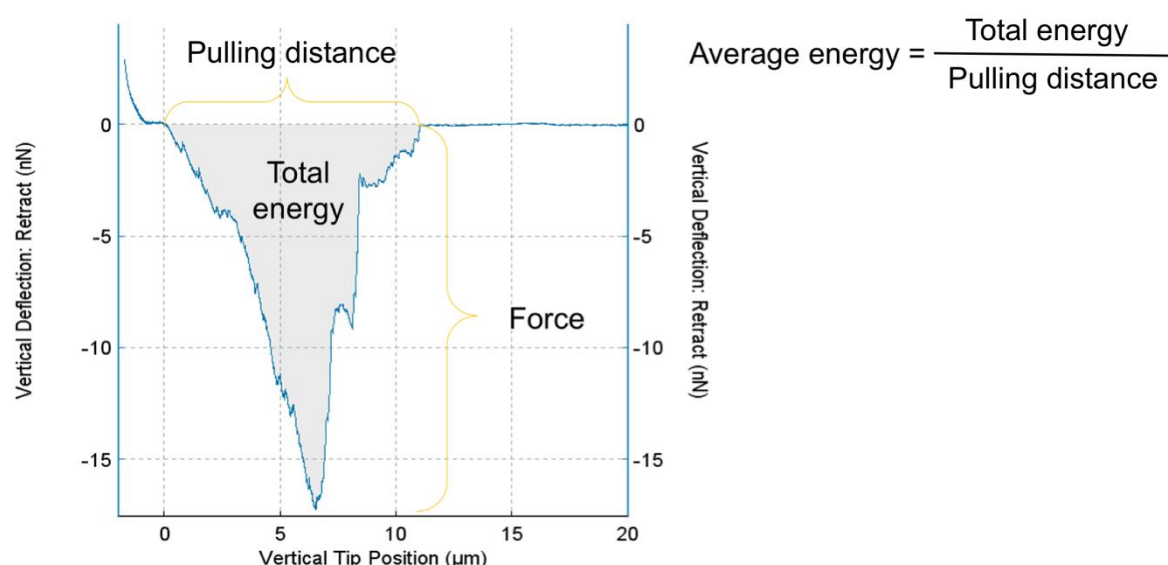
Figure 3 - Supplementary Figure 1. Analysis of the force and energy required to overcome the adhesion of *C. reinhardtii* flagella to the surface from AFM force curves.
The curve shows the relation of pulling force and pulling distance during AFM probe retracting. The lowest point of the curve represents the maximal adhesion force of flagella which was used in Figure 3C. The area of shaded region represents the total energy calculated by the JPK SPM Data Processing software for pulling up the cell. The average energy is calculated via dividing total energy by pulling distance as shown in the figure.
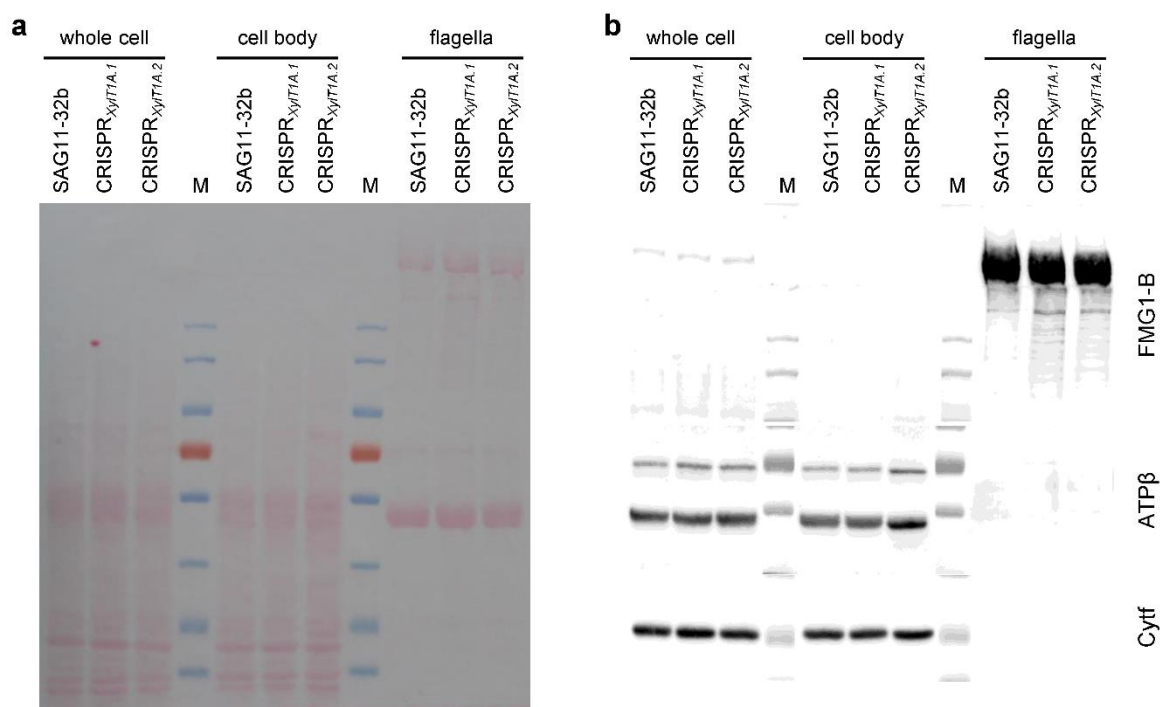
Figure 4 - Supplementary Figure 1. Xylosyltransferase 1A mutant generated via CRISPR/Cas9 supports findings in IM$_{XylT1A}$.

a, Schematic representation of the XylT1A gene including the site targeted by CIRSPR/Cas9. b, Parallel reaction monitoring was employed to prove the knock out of XylT1A on proteomic level in two mutants generated by CRISPR/Cas9. c, Comparison of *N*-glycan patterns between the XylT1A mutant strains in different genetic backgrounds (IM strain and CRISPR-Cas generated mutants) considering comparable *N*-glycosites. d, Detailed comparison of the *XylT1A* strains in different genetic background looking specifically at Pent (left), dHex (middle) and *N*-glycan length (number of Hex+MeHex, right).

Figure 4 - Supplementary Figure 2. Immunoblot proving the presence of FMG-1B in flagella of CRISPR$_{XylT1A.1}$ and CRISPR$_{XylT1A.2}$

30 µg of protein per sample were separated by SDS-PAGE and transferred to a nitrocellulose membrane in biological quadruplicates. a, Ponceau staining of the membrane reveals equal loading between different strains and differential composition of different sample types. b, On one hand, the FMG-1B protein backbone specific antibody proves a correct targeting of FMG-1B to flagella in the mutants despite altered N-glycosylation. On the other, the application of antibodies specifically binding to a chloroplast (Cytf, cytochrome f) marker protein as well as to the ATPase beta subunit (mitochondrial and chloroplast) proves the purity of flagellar samples analyzed.